Tuning Between Quantum-Dot- and Quantum-Well-Like Behaviors in Type II ZnTe Submonolayer Quantum Dots by Controlling Tellurium Flux During MBE Growth

H. Ji, B. Roy, S. Dhomkar, R. T. Moug, M. C. Tamargo, A. Wang & I. L. Kuskovsky

Journal of Electronic Materials

ISSN 0361-5235
Volume 42
Number 11

Journal of Elec Materi (2013)
42:3297-3302
DOI 10.1007/s11664-013-2729-2

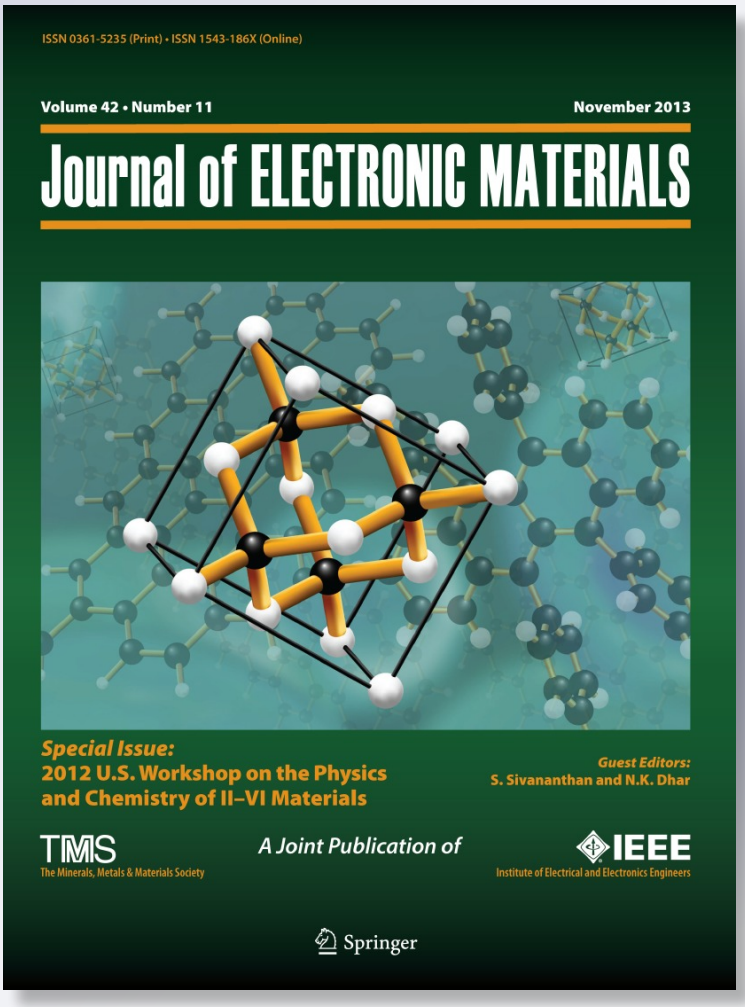

Springer

Journal of ELECTRONIC MATERIALS, Vol. 42, No. 11, 2013
DOI: 10.1007/s11664-013-2729-2

Tuning Between Quantum-Dot- and Quantum-Well-Like Behaviors in Type II ZnTe Submonolayer Quantum Dots by Controlling Tellurium Flux During MBE Growth

H. JI,[1,3,5] B. ROY,[1,3] S. DHOMKAR,[1,3] R.T. MOUG,[2] M.C. TAMARGO,[2,3] A. WANG,[4] and I.L. KUSKOVSKY[1,3]

1.—Queens College of CUNY, Flushing, NY 11367, USA. 2.—City College of CUNY, New York, NY 10031, USA. 3.—The Graduate Center of CUNY, New York, NY 10016, USA. 4.—Evans Analytical Group, Sunnyvale, CA 94086, USA. 5.—e-mail: hji1@qc.cuny.edu

We report tuning of properties of type II nanostructures between quantum dot (QD)-like and quantum well (QW)-like behaviors in ZnSe layers with ZnTe submonolayer insertions, grown by migration-enhanced epitaxy. The sizes of QDs are estimated from magneto-photoluminescence (PL) measurements, which showed no significant change in the QD lateral size with increasing Te flux, indicating increase in QD density instead. The area density of QDs is estimated from the results of secondary-ion mass spectrometry measurements. It is determined that, in the sample grown using the highest Te flux, the electronic wavefunctions begin to overlap, leading to QW-like behavior before the formation of a full QW layer. This is also confirmed via temperature-dependent time-resolved PL, which showed significant change of excitonic lifetimes and binding energies of type II excitons.

Key words: Type II heterostructures, submonolayer quantum dots, Zn-Se-Te, MBE, excitonic lifetime, quantum well

INTRODUCTION

Based on their band alignment, semiconductor heterostructures are generally divided into two types: type I heterostructures, where electrons and holes are located in the same material, which has lower potential for both of them, and type II heterostructures, where one of the materials has lower potential for electrons while the other has lower potential for holes, leading to spatial separation of the charge carriers. Because of the Coulomb interaction, these electrons and holes are bound in pairs, forming spatially indirect, type II, excitons. These excitons generally have recombination lifetimes longer than those of type I excitons. In addition, the energies and recombination oscillator strength of type II excitons are sensitive to the carrier densities as well as the external electric and magnetic fields.[1,2] These properties can be used for novel device applications.

Among type II semiconductor heterostructures, ZnSe layers with ZnTe submonolayer quantum dot (QD) multilayers have attracted a lot of interest due to the suitable band structure, which can be tuned to interact with light in a large wavelength range, from the ultraviolet to infrared.[2–4] For ZnTe QDs embedded in ZnSe barriers, photogenerated holes and electrons are located within the QDs and in the barriers, respectively.[2,3] Along with the fact that ZnTe can be easily doped *p*-type, this structure has practical applications in photodetectors[5] and photovoltaic devices.[6] Using a combination of migration-enhanced epitaxy (MEE) and molecular beam epitaxy (MBE), ZnTe submonolayer QDs can be grown *without* the formation of wetting layers, which might be key to improvements in device performance. Due to the low contrast between the ZnTe submonolayer QDs and ZnSe barriers, it is very difficult to characterize the structure by transmission electron microscopy. Therefore, indirect

(Received December 17, 2012; accepted August 13, 2013; published online September 4, 2013)

methods are required to finely probe the sizes and densities of the QDs.

For most device applications, the density of QDs is a very important parameter, since the degree of light absorption depends on it. With increasing QD density, it is expected that the QDs would start to coalesce, forming a quantum-well-like layer, which would change the electronic properties of the sample. For type II QDs, and for the ZnTe/ZnSe system in particular, where the electrons are located in the barriers, the wavefunctions of charge carriers can start to strongly overlap much earlier than the onset of physical QD coalescence. Thus, type II QD layers can start behaving like quantum wells (QWs) at much lower densities than those required for the formation of real QW layers, with obvious consequences for device performance. Herein, we report tuning between QD- and QW-like behaviors in ZnSe layers with ZnTe submonolayer QDs, by studying samples grown with increasing Te flux. Conditions and evidence for such tuning are obtained by measuring QD sizes and densities as well as analyzing photoluminescence (PL) spectra, and excitonic lifetimes and binding energies.

EXPERIMENTAL PROCEDURES

ZnSe layers with ZnTe submonolayer QDs were grown using a Riber 2300 MBE system on (001) GaAs substrates by a combination of MEE and MBE. Prior to the growth of the QD layers, an undoped ZnSe buffer layer was grown at optimum growth temperature of 270°C. After this, ZnSe layers with ZnTe QDs were grown following the same shutter sequence and steps as for the samples reported in Ref. 7. The ZnSe spacers between the QD layers were about 3.0 nm thick. By varying the Te cell temperature, three samples were grown using different Te fluxes during the formation of the QDs. All other growth conditions remained the same. The samples are listed in Table I, along with the total number of periods of the multilayers and the average Te concentration obtained via secondary-ion mass spectrometry (SIMS) performed by Evans Analytical Group. Samples A, B, and C are organized in order of increasing Te cell temperature.

For continuous-wave (cw) PL measurements, the 351-nm emission line from an Ar^+ laser was used for excitation. The emission was detected via a third stage of a TriVista SP2 500i triple monochromator coupled to a thermoelectrically cooled GaAs photomultiplier tube and a photon counting system. Samples were kept in an ARS Inc. temperature-variable closed-cycle refrigeration system, allowing for temperature-dependent measurements between 10 K and 300 K. The same cryosystem was used for the time-resolved PL (TRPL) measurements, where the 337-nm line of a N_2 pulsed laser with 4-ns pulse width was used for excitation, while a 500-MHz Tektronix TDS 654C oscilloscope was used for data

Table I. Sample parameters

Sample	Te Cell Temperature (°C)	Number of Periods	Te Concentration (atoms/cm^3)	Green Band Position at 50 K (eV)	Thickness of QDs (nm)	Electronic Orbit Radius (nm)	Area Density of QDs (cm^{-2})	Average Distance Between QD Centers (nm)
A	T_0	100	4.0×10^{19}	2.52	0.5	18.2	5.1×10^9	~140
B	$T_0 + 6$	250	6.5×10^{19}	2.51	0.5	18.7	8.0×10^9	~112
C	$T_0 + 60$	120	7.0×10^{20}	2.32	1.1	21.8	29.5×10^9	~58

T_0 relative temperature

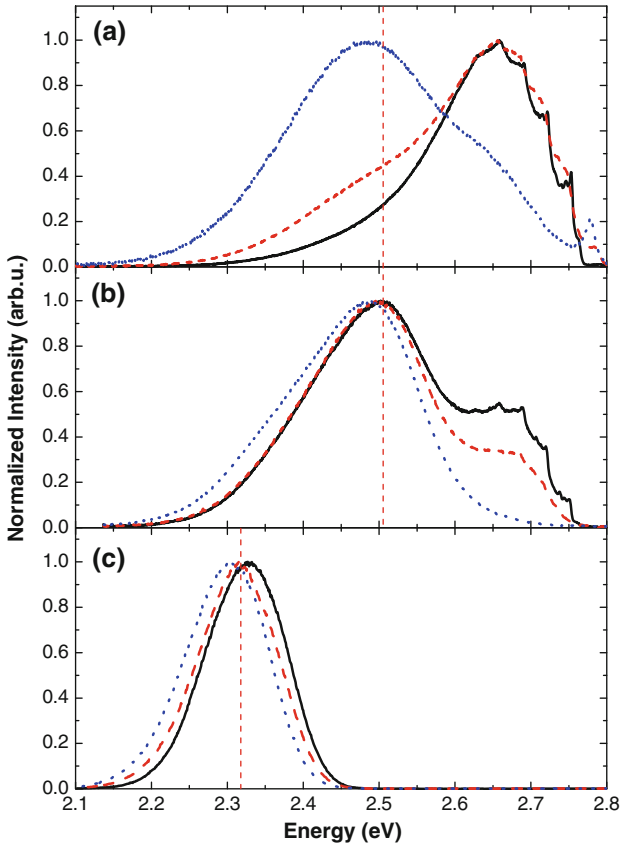

Fig. 1. Normalized PL at 10 K (black solid lines), 50 K (red dashed lines), and 90 K (blue dotted lines) for: (a) sample A, (b) sample B, and (c) sample C (Color figure online).

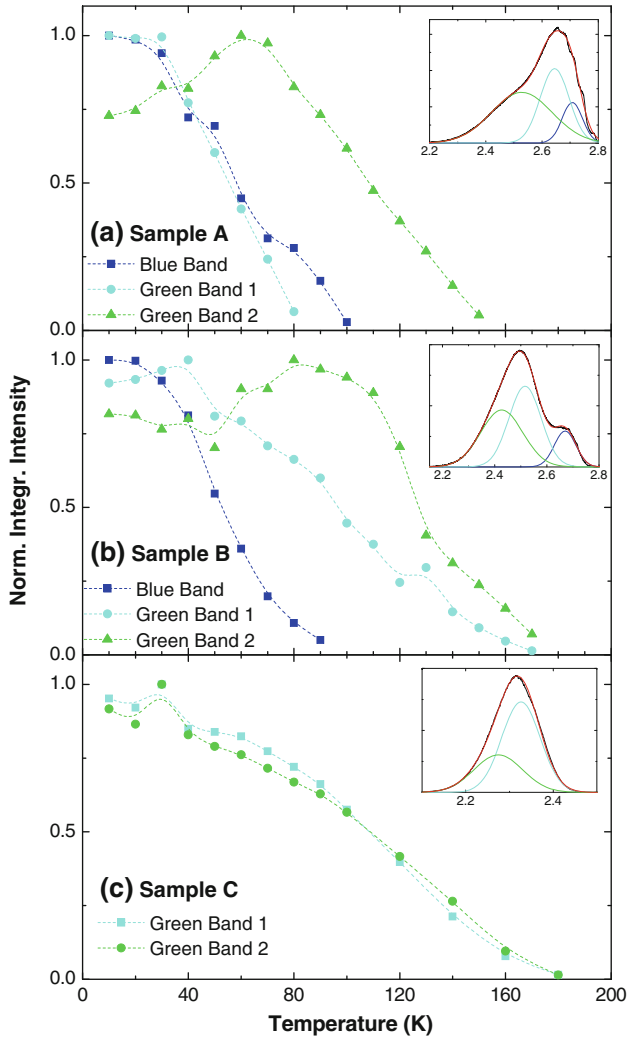

Fig. 2. Normalized integrated PL intensity as a function of temperature for: (a) sample A, (b) sample B, and (c) sample C. Insets show example fits of PL spectra at 50 K by Gaussian peaks.

recording. Magneto-PL measurements were performed within a Cryo Industries of America, Inc. 9-T superconducting magnet fitted with fiber-optic probes. In this case, the PL was excited by a 405-nm diode laser and detected with an Ocean Optics high-resolution solid-state spectrometer. The samples were cooled to 7.5 K by vaporizing liquid helium.

RESULTS AND DISCUSSION

The normalized PL spectra of all three samples for several measurement temperatures are shown in Fig. 1. It is apparent that each spectrum consists of several bands, and the relative intensities of these bands vary with the measurement temperature. We thus fit the spectra with Gaussian peaks, as shown in insets of Fig. 2 for the spectra at 50 K. The "green bands" (energy <2.6 eV) are related to type II ZnTe/ZnSe QDs, while the "blue bands" (energy >2.6 eV) are mostly related to $Te_{(n \geq 2)}$ isoelectronic centers (ICs) within the ZnSe barriers.[4] At 10 K, emission from ICs dominates in the spectrum of sample A, whereas the QD emission dominates in the spectrum of sample B. This implies that the density of QDs increases with the increase of Te flux during growth. There is no noticeable emission form ICs in the spectrum of sample C.

Considering the hole confinement in ZnTe QDs, one can estimate energy levels of the holes from the peak position of the green bands (listed in Table I). For this we interpolated the band parameters of ZnTe/ZnSe taken from Ref. 8 based on a 50% Te fraction within the QDs.[3] The obtained energy levels, measured from the top of the valence band of $ZnSe_{0.5}Te_{0.5}$, are 0.47 eV for samples A and B, and 0.28 eV for sample C. Since the lateral size of the submonolayer QDs is much larger than their thickness,[2] the energy level of holes is mostly determined by the confinement in the growth direction. We therefore numerically solved the Schrödinger equation for a hole in a one-dimensional QW to correlate the energy level of holes and the thickness of QDs. Using this approach, we determined the average thicknesses of the QDs for all the samples, also listed in Table I. The broadening of the green bands is related to the thickness distribution of QDs[4] and the electron–phonon

interaction.[9] The green band is narrower for sample C, indicating that the thickness distribution of the QDs is smaller in the sample grown with the highest Te flux (i.e., the QD sizes are more uniform).

The temperature dependences of the integrated PL intensity for the fit bands in the three samples are shown in Fig. 2. For samples A and B, as the temperature rises, the intensity of the blue band decreases, while the intensity of the green band increases up to ~80 K, decreasing thereafter. This is because of the competition between ICs and QDs. Excitons bound to ICs have lower binding energies than those bound to QDs. They start ionizing at lower temperature, and can become trapped at QDs, which enhances the emission from the latter while lowering the emission from ICs. When the temperature reaches ~80 K, the ionization process starts to dominate in both ICs and QDs, leading to the decrease of intensity for all bands. In sample C, due to the much higher density and more uniform size distribution of the QDs, an increase of temperature only contributes to the ionization, resulting in the immediate decrease of PL emission.

To estimate the radius of the type II QDs, one can use results of magneto-PL, as these dots exhibit the excitonic Aharonov–Bohm (AB) effect, as shown in Fig. 3. Analysis of the AB effect gives a direct and precise measure of the electronic orbit,[11] and therefore an estimation of the lateral size of the QDs.[10,11] Following the model of Refs. 10,11, we calculated the electronic orbit radius for these samples from the AB peak position, with the results listed in Table I. Comparing the electronic orbit radius with the average QD thickness for each sample, we find that, for higher Te flux during growth, the density of QDs increases: sample B has higher QD density than sample A, while the QD sizes are almost the same for both samples. For sample C, which has the highest Te flux, both the density and size of QDs increase compared with the other two samples. We further quantitatively estimated the area density of QDs, n_{QD}, as

$$n_{QD} = \frac{N_{Te}}{N_A}\left(\frac{h_L}{h_{QD}}\right)\frac{1}{\pi R^2 x}, \quad (1)$$

where N_{Te} is the average Te concentration as measured by SIMS, N_A is the volumetric atomic density of ZnTe, which is 3.52×10^{22} cm^{-3},[12] h_L and h_{QD} are the average thickness of one spacer layer and the QDs, respectively, R is the average radius of the QDs, which is about half the electronic orbit radius,[3,10,13] and $x \approx 0.5$ is the Te fraction within the QDs.[3,14] The results of this calculation are listed in Table I, along with the average distances between the centers of QDs as estimated from the area densities. Comparing the separation between QDs with the electronic orbit radius, the samples can be divided into two groups. For samples A and B, the average distance between QDs is about one order of magnitude larger than the electronic orbit radius, so that electrons bound to different QDs are not affected by each other. For sample C, the average distance between QDs is less than three times the electronic orbit radius. Therefore, it is possible

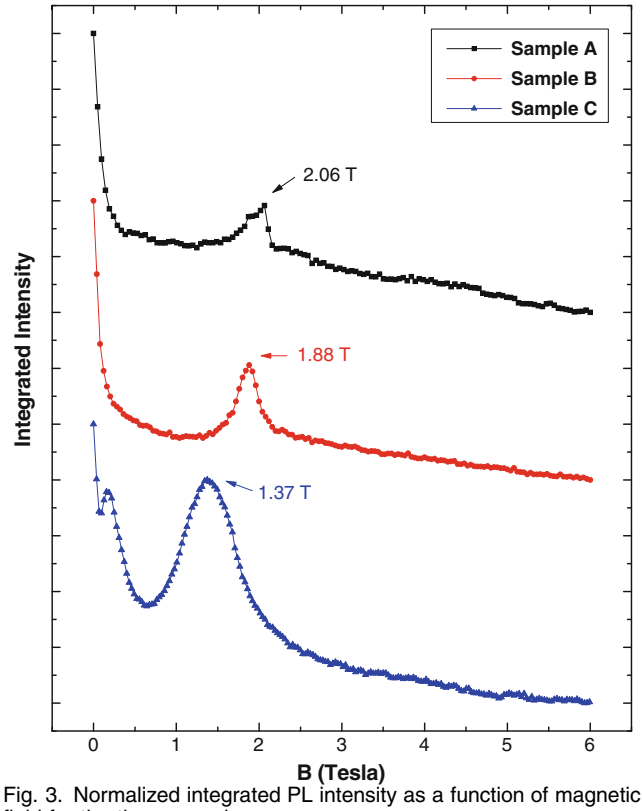

Fig. 3. Normalized integrated PL intensity as a function of magnetic field for the three samples.

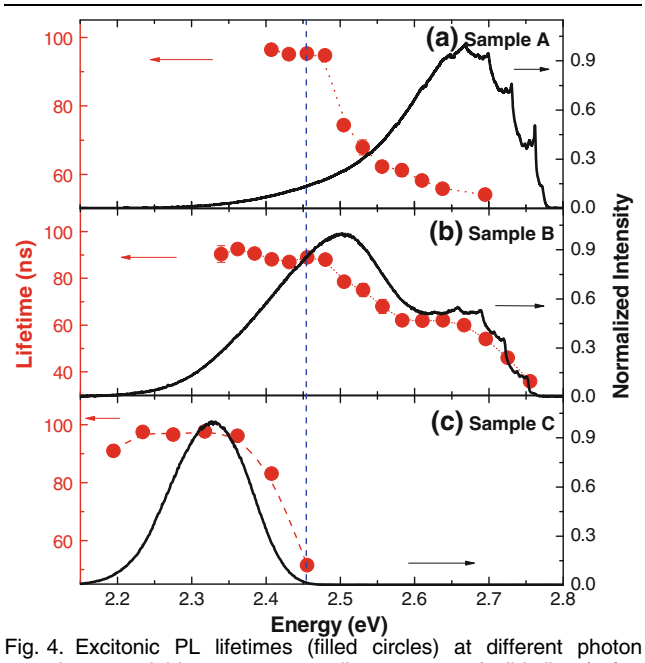

Fig. 4. Excitonic PL lifetimes (filled circles) at different photon energies, overlaid on corresponding spectra (solid lines) for: (a) sample A, (b) sample B, and (c) sample C.

that some electrons bound to neighboring QDs may have overlapping wavefunctions, leading to QW-like properties of the multilayers.

To further investigate this, we carried out temperature-dependent TRPL to extract the excitonic PL lifetimes and exciton binding energies. Figure 4 shows the excitonic PL lifetimes at low temperature across the spectra of the three samples. For samples A and B, at the higher energy side, the PL has relatively short lifetimes (~60 ns), since the emission is dominated by ICs. At the lower energy side, the PL lifetimes of all three samples approach similar values around 95 ns; these values give the lifetimes of excitons bound to type II ZnTe QDs at low temperature. We next consider emission at a photon energy of 2.45 eV, which is within the emission region associated with QDs, and find that the PL lifetime in sample C is ~52 ns, which is much shorter than that (~95 ns) for both sample A and sample B. We suggest that this is one of the effects of the overlapping of electron wavefunctions in sample C. Indeed, because of the vertical confinement in the multilayers with stacked QDs,[10] electrons prefer to be located in the barrier on the side of QDs, instead of above/below as for a single ideal QD.[2] In sample C, because some of the electron wavefunctions start to overlap, a fraction of the electrons might be located in the barrier region above/below the QDs, forming excitons like those in QW multilayers. Since the thickness of the submonolayer QDs is much smaller than their lateral size, these QW-like excitons have much stronger electron and hole wavefunction overlap, and therefore shorter lifetimes. In addition, due to the vertical confinement, the electrons located above/below QDs have higher energies than those located on the side of QDs. They contribute more on the higher energy side of the PL spectrum. Therefore, the excitonic lifetimes on the high-energy side are shorter than those on the low-energy side for sample C.

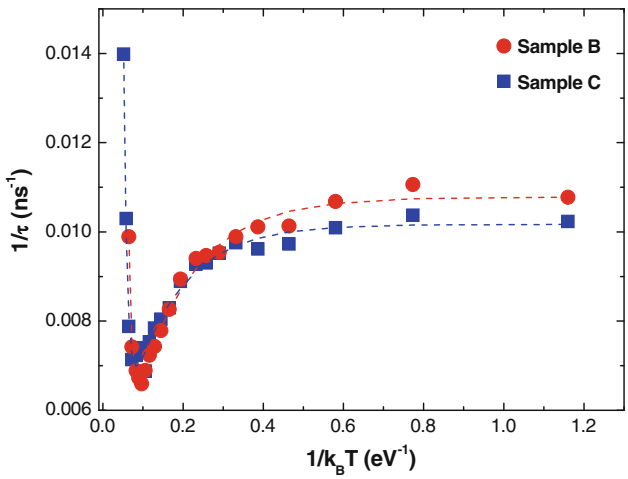

Fig. 5. Excitonic PL lifetimes as a function of temperature at 2.36 eV for sample B (red circles) and sample C (blue squares); dashed lines are fits to Eq. 2 (Color figure online).

We further consider the photon energy of 2.36 eV, which is only related to emission from QDs, for samples B and C, to study the dependence of excitonic PL lifetimes on temperature. Results are shown in Fig. 5. Within the temperature region below ~120 K, the excitonic lifetimes increase with increasing temperature, which is a signature of radiative recombination in type II QDs.[4] As the temperature rises, the weakly bound excitons are ionized, while the holes are still confined within the QDs, lowering the average overlap of wavefunctions of electrons and holes, which results in a longer lifetime of excitons undergoing radiative recombination. When temperature is higher than 120 K, the nonradiative processes of hole ionization[4] start to dominate. Thus, the excitonic lifetimes decrease with increasing temperature in the high-temperature region. It was argued in Ref. [4] that, under such conditions, the temperature dependence of a type II excitonic lifetime, τ, can be fitted with the following formula, first proposed in Ref. [15]:

$$\frac{1}{\tau} = \frac{1}{\tau_{r0}}[1 - C\exp(-\varepsilon_b/k_B T)] + \frac{1}{\tau_{nr0}}\exp(-\varepsilon_a/k_B T), \quad (2)$$

where C is a constant, k_B is the Boltzmann constant, τ_{r0} and τ_{nr0} are the radiative and nonradiative excitonic lifetimes at $T = 0$ K, respectively, ε_b is the exciton binding energy, and ε_a is the nonradiative activation energy. The fitting parameters with errors are listed in Table II. We notice that the exciton binding energy for sample C is comparatively larger than that in sample B, which is in conflict with the larger lateral QD size in sample C, if one assumes that in both samples electrons are located only at the "side" of all QDs.[7] This conflict, however, reveals the fact that, in sample C with high density of QDs, because of the overlapping of electron wavefunctions, a portion of the electrons

Table II. Fitting parameters of 2.36-eV type II excitons for samples B and C

Sample	Exciton Binding Energy (meV)	τ_{r0} (ns)	Nonradiative Activation Energy (meV)	τ_{nr0} (ns)
B	6.9 ± 0.3	93 ± 4	117.6 ± 10	0.10 ± 0.05
C	9.1 ± 0.9	99 ± 5	87.7 ± 5	1.21 ± 0.2

move to the barrier above/below the QDs, creating QW-like excitons which have stronger electron–hole overlap and therefore larger binding energies.

CONCLUSIONS

Combining SIMS, cw and TRPL, as well as magneto-PL measurements, we obtained the sizes and densities of type II ZnTe submonolayer QDs embedded in three ZnSe samples grown with different Te cell temperatures. We propose that, with increasing Te flux during growth, the density of QDs first increases without much change in the QD size. When the density of QDs becomes high enough that the electronic orbit radius is comparable to the average distance between QDs, some of the electron wavefunctions overlap with each other, resulting in a change of location of these electrons. Therefore, before the formation of full QW layers, a portion of the excitons bound to QDs start behaving like those in QW multilayers, showing characteristic properties such as shorter lifetimes and larger binding energies.

ACKNOWLEDGEMENTS

This work is supported by the National Science Foundation under Award No. DMR-1006050 and the Department of Energy, Office of Basic Energy Sciences, Division of Materials Sciences and Engineering under Award No. SC003739. Specifically, sample preparation, cw PL, and SIMS studies were carried out with DOE support (S.D., R.T.M., M.C.T., and I.L.K.), while the TRPL and the AB investigations were performed with support from the NSF (H.J., B.R., and I.L.K.). The authors are grateful to Prof. F. Cadieu and Dr. V. Shuvayev for helpful discussions and support.

REFERENCES

1. J.R. Madureira, M.P.F. de Godoy, M.J.S.P. Brasil, and F. Iikawa, *Appl. Phys. Lett.* 90, 212105 (2007).
2. I.L. Kuskovsky, W. MacDonald, A.O. Govorov, L. Mourokh, X. Wei, M.C. Tamargo, M. Tadic, and F.M. Peeters, *Phys. Rev. B* 76, 035342 (2007).
3. Y. Gong, W. MacDonald, G.F. Neumark, M.C. Tamargo, and I.L. Kuskovsky, *Phys. Rev. B* 77, 155314 (2008).
4. Y. Gu, I.L. Kuskovsky, M. van der Voort, G.F. Neumark, X. Zhou, and M.C. Tamargo, *Phys. Rev. B* 71, 045340 (2005).
5. J. Phillips, *J. Appl. Phys.* 91, 4590 (2002).
6. A. Luque and A. Marti, *Adv. Mater.* 22, 160 (2010).
7. B. Roy, A.D. Shen, M.C. Tamargo, and I.L. Kuskovsky, *J. Electron. Mater.* 40, 1775 (2011).
8. V.A. Shuvayev, I.L. Kuskovsky, L.I. Deych, Y. Gu, Y. Gong, G.F. Neumark, M.C. Tamargo, and A.A. Lisyansky, *Phys. Rev. B* 79, 115307 (2009).
9. I.L. Kuskovsky, Y. Gong, G.F. Neumark, and M.C. Tamargo, *Superlattice Microst.* 47, 87 (2010).
10. B. Roy, H. Ji, S. Dhomkar, F.J. Cadieu, L. Peng, R. Moug, M.C. Tamargo, Y. Kim, D. Smirnov, and I.L. Kuskovsky, *Phys. Rev. B* 86, 165310 (2012).
11. B. Roy, H. Ji, S. Dhomkar, F.J. Cadieu, L. Peng, R. Moug, M.C. Tamargo, and I.L. Kuskovsky, *Appl. Phys. Lett.* 100, 213114 (2012).
12. S. Larramendi, F.C. Zawislak, M. Behar, E. Pedrero, M.H. Velez, and O. de Melo, *J. Cryst. Growth* 312, 892 (2010).
13. K.L. Janssens, B. Partoens, and F.M. Peeters, *Phys. Rev. B* 64, 155324 (2001).
14. Y. Gong, H.F. Yan, I.L. Kuskovsky, Y. Gu, I.C. Noyan, G.F. Neumark, and M.C. Tamargo, *J. Appl. Phys.* 99, 064913 (2006).
15. J.D. Cuthbert and D.G. Thomas, *Phys. Rev.* 154, 763 (1967).